A Bi-Directional DC/DC Converter for an Energy Storage System

Shigenori Inoue, *Student Member*, *IEEE*, and Hirofumi Akagi, *Fellow*, *IEEE*
Department of Electrical and Electronic Engineering
Tokyo Institute of Technology
S3-17, 2-12-1, O-okayama, Meguro, Tokyo, 152-8552, JAPAN
E-mail: inoue@akg.ee.titech.ac.jp, akagi@ee.titech.ac.jp

***Abstract*— This paper addresses a bi-directional dc/dc converter suitable for an energy storage system with an additional function of galvanic isolation. An energy storage device such as an electric double layer capacitor is directly connected to one of the dc buses of the dc/dc converter without any chopper circuit. Nevertheless, the dc/dc converter can continue operating when the voltage across the energy storage device droops along with its discharge. Theoretical calculation and experimental measurement reveal that power loss and peak current impose limitations on a permissible dc-voltage range. This information may be useful in design of the dc/dc converter. A laboratory model of the energy storage system rated at 200 V and 2.6 kJ designed and constructed in this paper verifies that the dc/dc converter can charge and discharge the capacitor bank properly. Moreover, the dc/dc converter can charge the capacitor bank from zero to the rated voltage without any external precharging circuit.**

I. Introduction

Generally, electric power generated by renewable energy sources is unstable in nature, thus producing a bad effect on the utility grid. This fact spurs research on energy storage systems to smooth out active-power flow on the utility grid [1], [2]. Fig. 1 shows a conventional energy storage system employing a line-frequency (50- or 60-Hz) transformer, a PWM converter, a bi-directional chopper, and an energy storage device such as electric double layer capacitors (EDLCs) or lithium-ion batteries. The transformer is indispensable for some applications that require voltage matching and/or galvanic isolation between the utility grid and the energy storage device. Replacing the line-frequency transformer with a high-frequency and isolated dc/dc converter would result in a more compact and flexible energy storage system.

Various bi-directional isolated dc/dc converters have been proposed as the interface to energy storage devices with focus on automotive or fuel cell applications. Most of the presented dc/dc converters have asymmetrical circuit configurations to couple the two dc buses having largely different voltages, several tens volts and several hundreds volts [3]-[9].

Fig. 2 depicts a bi-directional isolated dc/dc converter presented in 1991 [10], [11]. It had two symmetrical single-phase voltage-fed full-bridge converters. The dc/dc converter suffered from a low efficiency because the first-generation IGBTs were used as switching power devices [10]. However, advancement in power device technology over the last decade has enabled the dc/dc converter to operate at an efficiency as high as 97% [12]. A resonant dc/dc converter based on the similar topology has also achieved the same efficiency [13]. In addition, when the SiC power devices become available in the near future, the efficiency of the dc/dc converter in Fig. 2 may reach 99%. Therefore, the dc/dc converter in Fig. 2 has become a promising candidate as a power electronic interface for an energy storage system.

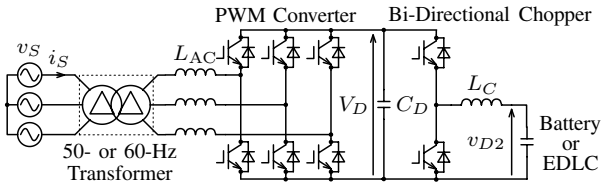

Fig. 1. A conventional energy storage system employing a 50- or 60-Hz transformer.

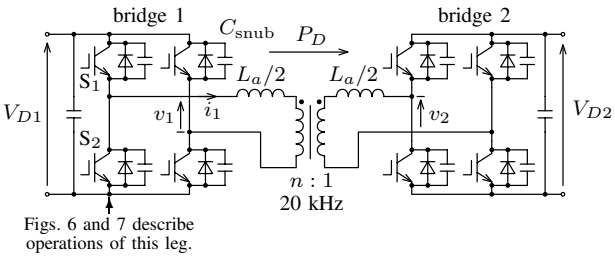

Fig. 2. A bi-directional isolated dc/dc converter.

Fig. 3 shows the energy storage system using the bi-directional isolated dc/dc converter in Fig. 2. Appropriately choosing the transformer turn ratio n enables to design the voltage range of the energy storage device, independent of the utility voltage. The energy storage device is directly connected to one of the dc buses of the dc/dc converter without any chopper circuit. Nevertheless, the dc/dc converter continues operating even when the voltage across the energy storage device, V_{D2} droops along with its discharge.

However, no paper has addressed the permissible voltage range of V_{D2} in terms of power loss and peak current. There has been no experimental verification based on the dc/dc converter. This paper analyzes the relationships between the power loss, the peak current, and V_{D2} in a dc/dc converter rated at 10 kW and 20 kHz with V_{D1} fixed to 320 V. Then, the dc/dc converter is constructed and experimentally tested to

1-4244-0714-1/07/$20.00 ©2007 IEEE.

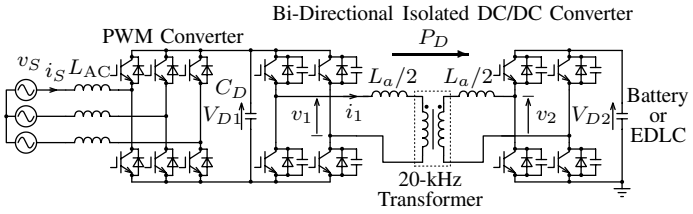

Fig. 3. An energy storage system based on the bi-directional isolated dc/dc converter.

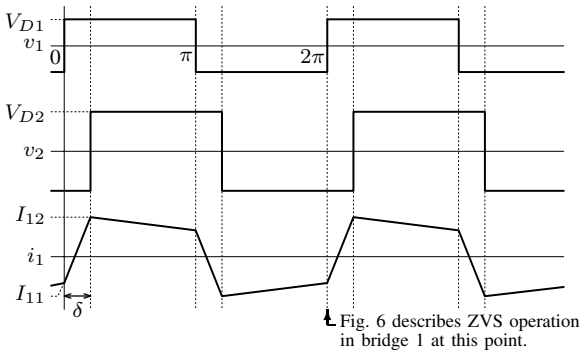

Fig. 4. Simplified theoretical waveforms used to analyze the power losses when $V_{D1} < V_{D2}$.

verify the analysis. A 2.6-kJ laboratory model of the energy storage system using an electrolytic capacitor bank, together with the dc/dc converter, demonstrates stable charging and discharging operation. Besides, the dc/dc converter can charge the capacitor bank from zero to the rated voltage without any external precharging or starting-up circuit.

II. The Bi-Directional Isolated DC/DC Converter

A. Operation Principle and Simplified Theoretical Waveforms

Fig. 4 illustrates simplified theoretical waveforms of the dc/dc converter where $V_{D1} < V_{D2}$. The two single-phase voltage-fed full-bridge converters produce square voltages v_1 and v_2. The power transfer P_D can simply be controlled by adjusting the phase shift between v_1 and v_2, δ as expressed by [10]

$$P_D = \frac{V_{D1}V_{D2}}{\omega L}\left(\delta - \frac{\delta^2}{\pi}\right), \tag{1}$$

where ω $(= 2\pi f)$ is the switching angular frequency of the two single-phase voltage-fed full-bridge converters, and L is the sum of the transformer leakage inductance $L_{\rm trans}$ and the inductance of the auxiliary inductors L_a.

As can be seen in Fig. 4, this paper defines a set of two instantaneous values of the current i_1 as "switching currents," I_{11} and I_{12} which are calculated as

$$I_{11} = -\frac{(V_{D1}+V_{D2})\delta + (V_{D1}-V_{D2})(\pi-\delta)}{2\omega L} \tag{2}$$

and

$$I_{12} = \frac{(V_{D1}+V_{D2})\delta - (V_{D1}-V_{D2})(\pi-\delta)}{2\omega L}. \tag{3}$$

I_{11} and I_{12} are the instantaneous values of i_1 when v_1 and v_2 respectively change their polarity from negative to positive.

In this paper, a single-phase voltage-fed full-bridge converter is referred to simply as a "bridge." In the following experiments, the transformer turn ratio is unity $(n = 1)$ for the sake of simplicity.

B. An Experimental Circuit of the DC/DC Converter

Table I summarizes the circuit parameters of the dc/dc converter. Four auxiliary inductors, totally having $L_a = 40$ μH, are connected in series with the transformer to obtain an inductance of $L = 41.6$ μH together with the leakage inductance of the transformer, $L_{\rm trans}$. The inductance of 41.6 μH is sufficient to maintain a control resolution of power transfer around 120 W because the time resolution of the controller is 50 ns that corresponds to 0.36° at 20 kHz.

TABLE I

Circuit Parameters of the DC/DC Converter.

Rated power		10 kW
Rated DC voltage	V_{D1}, V_{D2}	360 V
DC capacitor	C_D	7,100 μF
Unit capacitance constant	H	46 ms
Transformer core material		Finemet FT-3M
Transformer turn ratio		1 : 1
Transformer leakage inductance	$L_{\rm trans}$	1.6 μH (1.6%)
Transformer winding resistance	$R_{\rm trans}$	17 mΩ (0.13%)
Auxiliary inductor	$L_a/2$	21 μH (19%)
Auxiliary inductor core material		Ferrite (PC44)
Inductor winding resistance	$R_a/2$	20 mΩ (0.15%)
Snubber Capacitor	$C_{\rm snub}$	0.01 μF (1.6%)
Switching Frequency	f	20 kHz

Based on single-phase 360 V, 10 kW, and 20 kHz.

The following sections analyze relationships between power transfer and power losses in the dc/dc converter. The power losses depend not only on the power transfer, but also the dc voltage V_{D2}. When V_{D2} droops along with discharge of the energy storage device, power loss increases at a given power transfer.

III. Snubber Loss

A. Operating Points and ZVS Conditions

In Fig. 2, a snubber capacitor $C_{\rm snub}$ is connected in parallel with each IGBT both to reduce switching loss and to damp out overvoltage. If the IGBT is turned on with its snubber capacitor charged, the capacitor is shorted out by the IGBT, and the energy stored in the capacitor is dissipated, thus resulting in power loss. This paper refers to this power loss as "snubber loss."

When both dc voltages are equal $(V_{D1} = V_{D2})$, and the power transfer is sufficiently large around its rating, each IGBT is turned on in ZVS (zero-voltage switching) manner to generate no snubber loss. However, when $V_{D1} \neq V_{D2}$, and the power transfer is small, the IGBT is not necessarily turned on in ZVS manner.

Fig. 5 shows simplified theoretical waveforms when the IGBTs in bridge 1 is turned on in hard-switching manner.

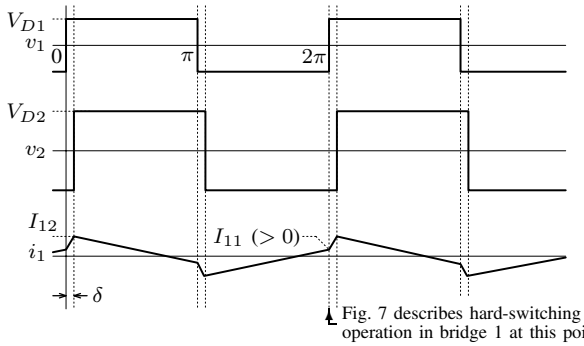

Fig. 5. Waveforms when a positive I_{11} forces bridge 1 to operate in hard-switching manner.

The power transfer is less than that in Fig. 4 although the dc voltages V_{D1} and V_{D2} are the same as those in Fig. 4. The switching current I_{11} is now positive in Fig. 5 in contrast to negative I_{11} in Fig. 4. With a positive I_{11}, the so-called "reverse recovery" occurs in the free-wheeling diodes in bridge 1, leading to hard-switching operation. Turn-on operations of the IGBTs in bridge 1 and bridge 2 can be classified into the following three: (1) ZVS operation, (2) incomplete ZVS operation, and (3) hard switching operation, depending on the phase shift δ, the dc voltages V_{D1} and V_{D2}, and the dead time T_d. The incomplete ZVS and hard-switching operations can take place only in one bridge whose dc voltage is lower than the other. Therefore, the four IGBTs in bridge 2 are turned on in ZVS manner because $V_{D1} < V_{D2}$. The following calculations mainly focus on phenomena in bridge 1 because those in bridge 2 can be described alike.

B. Calculations of the Snubber Loss

1) ZVS operation: Fig. 6 shows circuit modes when a leg in bridge 1 (for example, consisting of S_1 and S_2) operates in ZVS manner. Before the dead time, a current of I_{11} is flowing in S_2 (see Fig. 6(a)). When S_2 is turned off, the dead time starts. The current flowing in S_2 commutates to the snubber capacitors $C_{\rm snub1}$ and $C_{\rm snub2}$. Resonance between the inductance L (see Fig. 2), $C_{\rm snub1}$, and $C_{\rm snub2}$ begins. $C_{\rm snub1}$ discharges from V_{D1} to zero while $C_{\rm snub2}$ charges from zero to V_{D1}. The energy stored in $C_{\rm snub1}$ is transferred to $C_{\rm snub2}$. When $C_{\rm snub1}$ discharges down to zero, the current commutates to D_1 (see Fig. 6(c)). An amount of energy stored in L is regenerated back to V_{D1} through D_1. Providing a gating signal while D_1 is conducting can turn S_1 on in ZVS manner. This operation results in no snubber loss.

2) Incomplete ZVS Operation: IGBTs in bridge 1 can not necessarily be turned on in ZVS manner even with a negative I_{11}. If the magnitude of I_{11}, or $|I_{11}|$ is smaller than $I_{\rm min}$, $C_{\rm snub1}$ is not discharged down to zero, and $C_{\rm snub2}$ is not charged up to V_{D1} where [11]

$$I_{\rm min} = \frac{2\sqrt{V_{D1}V_{D2}}}{Z_r} \tag{4}$$

and

$$Z_r = \sqrt{\frac{L}{C_{\rm snub}}}. \tag{5}$$

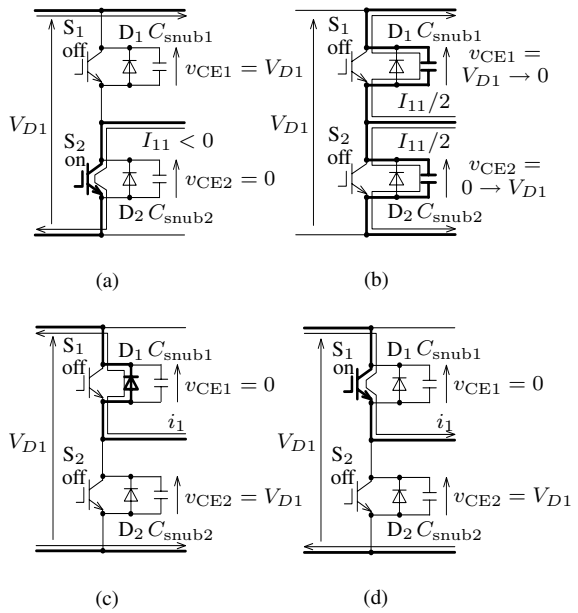

Fig. 6. ZVS on a leg in bridge 1: (a) just before the dead time starts, (b) just after the dead time starts, (c) diode free wheeling, (d) current polarity alternates after the dead time.

In this case, the operation of the leg makes a direct transition from Fig. 6(b) to (d), not through (c). Turning S_1 on with $C_{\rm snub1}$ charged results in an amount of snubber loss. This paper refers to this as "incomplete ZVS operation."

Snubber loss caused by incomplete ZVS operation can be calculated as follows. The collector-emitter voltage of S_1, $v_{\rm CE1}$ in Fig. 6(b) can be expressed as

$$v_{\rm CE1}(t) = \frac{(V_{D1}+V_{D2}) + (V_{D1}-V_{D2})\cos\omega_r t}{2} - \frac{Z_r|I_{11}|\sin\omega_r t}{2}, \tag{6}$$

where t is the time after the beginning of the dead time, and ω_r $(= 1/\sqrt{LC_{\rm snub}})$ is the resonant angular frequency of $C_{\rm snub}$ and L. At the end of the dead time ($t = T_d$), $v_{\rm CE1}(T_d)$ is not zero beacuse $|I_{11}| < I_{\rm min}$. $C_{\rm snub1}$ is shorted out and quickly discharges from $v_{\rm CE1}(T_d)$ to zero. $C_{\rm snub2}$ suddenly charges from $V_{D1} - v_{\rm CE1}(T_d)$ to V_{D1}. As a result, a joule loss of

$$W_{\rm snub} = C_{\rm snub}\{v_{\rm CE1}(T_d)\}^2 \tag{7}$$

is dissipated in S_1, where $C_{\rm snub} = C_{\rm snub1} = C_{\rm snub2}$. Note that charging $C_{\rm snub2}$ as well as discharging $C_{\rm snub1}$ contributes to the joule loss. $W_{\rm snub}$ represents an amount of energy lost at one switching per leg. The snubber loss $P_{\rm snub}$ in bridge 1, having two legs, is calculated as

$$P_{\rm snub} = 4 \cdot f \cdot W_{\rm snub} = 4 \cdot f \cdot C_{\rm snub}\{v_{\rm CE1}(T_d)\}^2. \tag{8}$$

3) Hard-Switching Operation: Fig. 7 shows circuit modes when the leg operates in hard-switching manner. If $V_{D1} < V_{D2}$, and the following equation is satisfied, the switching

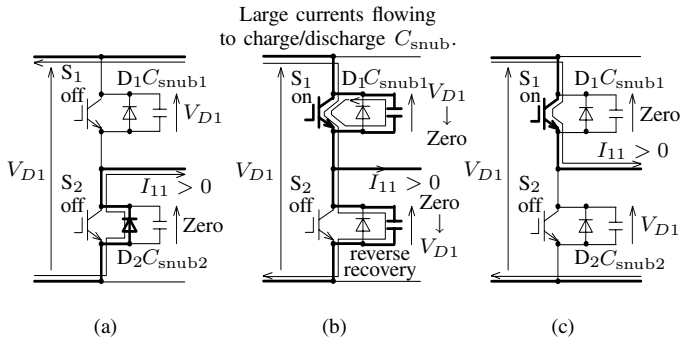

Fig. 7. Hard switching on a leg in bridge 1: (a) just before the dead time ends, (b) rapid charging/discharging of $C_{\rm snub1}$ and $C_{\rm snub2}$, (c) after commutation.

current I_{11} becomes positive, and the IGBTs in bridge 1 are turned on in hard-switching manner: [10]

$$\delta \le \frac{V_{D2} - V_{D1}}{2V_{D2}}\pi. \tag{9}$$

Before the end of the dead time, $C_{\rm snub1}$ is charged at V_{D1} (see Fig. 7(a)). Just after S_1 is turned on, reverse recovery occurs in D_2. $C_{\rm snub1}$ rapidly discharges from V_{D1} to zero, and $C_{\rm snub2}$ charges from zero to V_{D1} (see Fig. 7(b)). The charging/discharging currents result in a joule loss of $W_{\rm snub} = C_{\rm snub}V_{D1}^2$ in S_1. Then, the snubber loss $P_{\rm snub}$ in bridge 1 is calculated as

$$P_{\rm snub} = 4 \cdot f \cdot W_{\rm snub} = 4 \cdot f \cdot C_{\rm snub}V_{D1}^2. \tag{10}$$

As can be seen in (8) and (10), the snubber loss $P_{\rm snub}$ is proportional to the capacitance of the snubber capacitors $C_{\rm snub}$. Minimizing parasitic inductances in the dc/dc converter circuit is necessary so that small snubber capacitors can damp out the overvoltage appearing across the IGBTs without causing an excessive snubber loss.

IV. Profile of the Current i_1 and Related Losses

A. Conducting Loss in the IGBTs

This paper approximates both the on-state voltage across the IGBT, $V_{\rm CE(sat)}$, and the forward voltage drop across the free-wheeling diode, V_F, to be 1.5 V, independently of the current flowing in them [12]. The conducting loss in the IGBTs and diodes, $P_{\rm cond}$ can be calculated from the average of the absolute value of the current i_1, or $\langle|i_1|\rangle$.

When both bridge 1 and bridge 2 is operated in ZVS or incomplete ZVS manner, calculation on Fig. 4 yields

$$\langle|i_1|\rangle = \frac{V_{D1}V_{D2}}{\omega L(V_{D1}+V_{D2})}\left\{-\frac{\delta^2}{\pi} + 2\delta + \frac{\pi(V_{D1}-V_{D2})^2}{4V_{D1}V_{D2}}\right\}. \tag{11}$$

On the other hand, when either bridge 1 or bridge 2 is operated in hard-switching manner, calculation on Fig. 5 derives:

$$\langle|i_1|\rangle = \frac{1}{\omega L}\left\{\frac{V_{D1}V_{D2}}{|V_{D1}-V_{D2}|}\frac{\delta^2}{\pi} + |V_{D1}-V_{D2}|\frac{\pi}{4}\right\}. \tag{12}$$

To calculate $\langle|i_1|\rangle$, I_{11} and I_{12} should be obtained first, and then either (11) or (12) should be applied, depending on the switching manner.

B. Copper Loss in the Transformer and the Inductors

The rms value of i_1, or I_1 can be expressed by

$$I_1 = \frac{\sqrt{V_{D1}V_{D2}}}{\omega L}\sqrt{-\frac{4}{3\pi}\delta^3 + \delta^2 + \frac{\pi^2}{12}\frac{(V_{D1}-V_{D2})^2}{V_{D1}V_{D2}}}, \tag{13}$$

regardless of the switching manner. The copper loss in the transformer and the auxiliary inductors, $P_{\rm copp}$ is obtained as

$$P_{\rm copp} = (R_{\rm trans} + R_a) \cdot I_1^2, \tag{14}$$

where $R_{\rm trans} = 17$ mΩ is the winding resistance of the transformer, and $R_a = 40$ mΩ is that of the auxiliary inductors.

C. Core Loss in the Auxiliary Inductors

The four auxiliary inductors were constructed using ferrite (TDK PC44) cores. The effective cross-sectional area of each core was $A_e = 3.3$ cm^2, the effective volume was $V_e = 37.2$ cm^3, and the turn number was $N = 6$. An air gap of $g = 1.5$ mm was introduced in the magnetic path. Thus, the instantaneous magnetic flux density $b_{\rm ind}$ is approximately expressed as

$$b_{\rm ind} \simeq \frac{\mu_0}{g}Ni_1, \tag{15}$$

where μ_0 is the permeability of vacuum. The datasheet of PC44 indicates that its core loss per volume is 0.6 W/cm^3 when the maximum flux density is 0.2 T at a frequency of 100 kHz in a temperature of 25°C. If the core loss per volume in PC44 can be approximated by kfB^2, where f is the frequency of magnetization, the coefficient $k = 0.15$ mW/HzT^2. This paper assumes that a 20-kHz sinusoidal current having an rms value as large as I_1 is responsible for the core loss in the auxiliary inductors. Under this assumption, the core loss in the four auxiliary inductors can be calculated as

$$P_{\rm core(ind)} = 4kf\left(\frac{\mu_0}{g}N\sqrt{2}I_1\right)^2 V_e = \frac{8kf\mu_0^2N^2V_e}{g^2}I_1^2, \tag{16}$$

where $\sqrt{2}$ is the coefficient to transform an rms value into an amplitude. Therefore, the core loss in the auxiliary inductors can be treated as an equivalent winding resistance of

$$R_{\rm core(ind)} = \frac{8kf\mu_0^2N^2V_e}{g^2} = 23\ {\rm m}\Omega. \tag{17}$$

The core loss in the auxiliary inductors can be calculated as a part of copper loss.

V. Power Losses and Lower Limit of V_{D2}

A. Comparison between Theoretical and Experimental Losses

Theoretical losses described above are compared to measurement results on the basis of an experimental dc/dc converter rated at 10 kW and 20 kHz. The circuit configuration and the circuit parameters are the same as those in Fig. 2 and Table I, respectively. A regulated dc power supply is connected to the dc bus of bridge 1. The dc bus of bridge 2 is connected back to that of bridge 1 so that the transferred power can be regenerated back to the dc power supply. Thus, the power

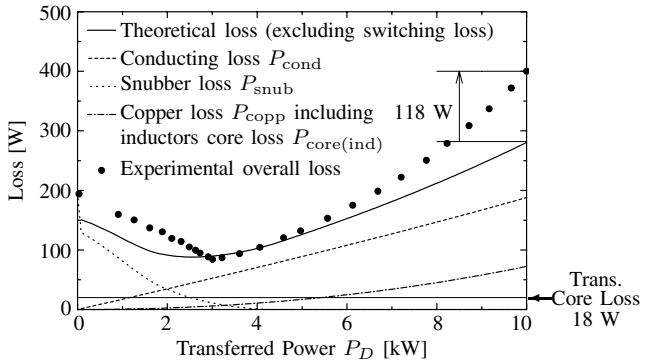

Fig. 8. Comparison between calculated and experimental power losses at $V_{D1} = V_{D2} = 350$ V.

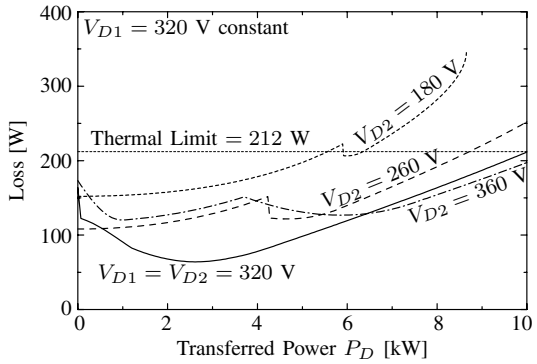

Fig. 9. Sum of theoretical conducting and snubber losses ($P_{\rm cond} + P_{\rm snub}$) when P_D is positive.

coming from the dc power supply equals the overall loss in the dc/dc converter. Both theoretical calculation and measurement are carried out under $V_{D1} = V_{D2} = 350$ V.

Fig. 8 shows comparisons between the theoretical and experimental losses. The solid line corresponds to the theoretical overall loss, $P_{\rm theory}$ although it excludes the switching loss in the IGBTs, or $P_{\rm sw}$. When $P_D = 10$ kW, the theoretical losses were as follows. The conducting loss was $P_{\rm cond} = 189$ W. The snubber loss was $P_{\rm snub} = 0$ W. The copper loss both in the transformer and the inductors $P_{\rm copp} = 73$ W including the core loss in the inductors, $P_{\rm core(ind)}$. The core loss in the transformer was $P_{\rm core(tr)} = 18$ W almost independently of the power transfer. The theoretical overall loss $P_{\rm theory}$ was 282 W.

The experimental value of the overall loss, on the other hand, was 400 W. Thus, the difference between the theoretical and measurement results were 118 W. It would correspond to the switching loss in the IGBTs that was excluded from the theoretical overall loss. In [12], the switching loss in the IGBTs was 90 W when a power of 10 kW was transferred. Although the error of $118^{\rm W} - 90^{\rm W} = 28$ W remains unidentified, the theoretical calculations above can be valid because the error of 28 W corresponds to 0.28% of the power transfer of 10 kW, and 7% of the measured overall loss of 400 W.

B. Thermal Limit and V_{D2}

Fig. 9 shows theoretical calculation results of conducting and snubber losses in the IGBTs ($P_{\rm cond} + P_{\rm snub}$) when the power transfer P_D is positive. In Fig. 9, one dc voltage V_{D1} was kept constant at 320 V, while the other dc voltage V_{D2} was changed as a parameter.

Achieving ZVS operation becomes difficult with $V_{D1} \neq V_{D2}$, compared to $V_{D1} = V_{D2} = 320$ V, resulting in an increased snubber loss around 3 kW.

Fig. 9 defines $P_{\rm cond} + P_{\rm snub} = 212$ W at $V_{D1} = V_{D2} = 320$ V as a "thermal limit." In the dc/dc converter, the losses in the IGBTs, which are the most dominant in the overall loss, may make the IGBT modules mounted on a heatsink suffer from the highest temperature. The temperature of the IGBT modules, more precisely semiconductor dies in the modules, determines the maximum power transfer. Therefore, this paper considers only the losses in the IGBTs as the thermal limit.

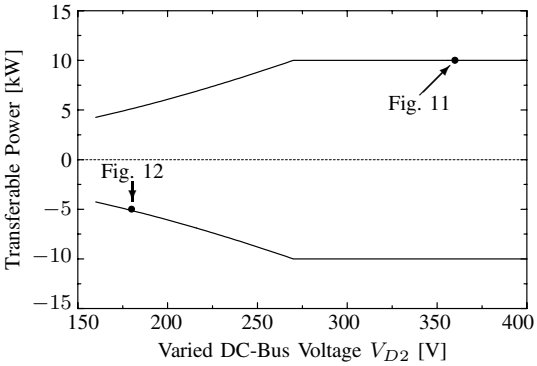

Fig. 10. Transferable powers when limiting the peak value of current i_1 under 60 A, and their operating points in experiments.

When $V_{D2} = 180$ V, the losses in the IGBTs exceed the thermal limit at $P_D > 5.6$ kW. Hence, when $V_{D2} = 180$ V, the dc/dc converter has to operate under 5.6 kW. When $V_{D2} = 260$ V, the losses in the IGBTs exceed the thermal limit at $P_D > 8.6$ kW. Hence, when $V_{D2} = 260$ V, the dc/dc converter has to operate under 8.6 kW.

VI. Peak Current in the Auxiliary Inductors

The ferrite cores in the auxiliary inductors would get magnetically saturated if the current i_1 exceeds 60 A because the magnetic flux density reaches 0.3 T as calculated by (15). The dc/dc converter has to be operated under the limitation on the peak value of i_1, or $I_{\rm 1peak}$. The peak current imposes limitations on the dc voltage V_{D2}. When $V_{D1} > V_{D2}$, the peak current $I_{\rm 1peak}$ equals I_{11}. When $V_{D1} < V_{D2}$, the peak current $I_{\rm 1peak}$ equals I_{12}.

Fig. 10 shows maximum transferable power when the peak current $I_{\rm 1peak}$ is limited under 60 A. Solid dots "•" indicate the operating points of the waveforms shown below. When $V_{D2} = 180$ V, $I_{\rm 1peak}$ exceeds 60 A at $P_D = 5.1$ kW. When $V_{D2} = 260$ V, $I_{\rm 1peak}$ exceeds 60 A at $P_D = 9.4$ kW.

As has been stated above, both the power loss and the peak current impose limitations on the power transfer P_D and the dc voltage V_{D2}. Operation of the dc/dc converter has to satisfy both limitations.

Fig. 11 shows the experimental waveforms when one dc voltage is 320 V while the other is 360 V at $P_D = 10$ kW

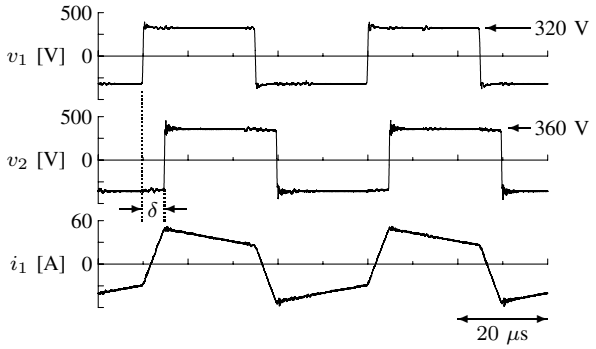

Fig. 11. Experimental waveforms when $V_{D1} = 320$ V, $V_{D2} = 360$ V, $\delta = 35°$, and $P_D = 10$ kW.

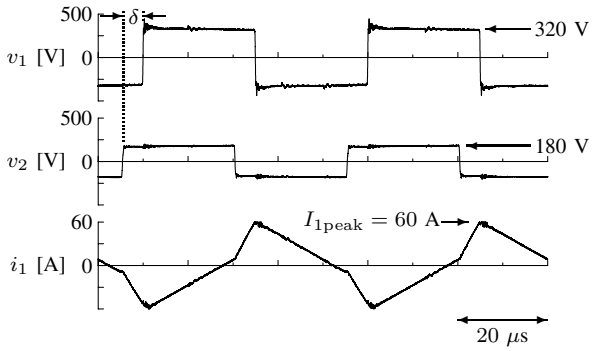

Fig. 12. Experimental waveforms when $V_{D1} = 320$ V, $V_{D2} = 180$ V, $\delta = -41°$, and $P_D = -5$ kW.

from bridge 1 to 2. Fig. 12 shows another example of the experimental waveforms which was taken when $V_{D1} = 320$ V while $V_{D2} = 180$ V at $P_D = 5$ kW from bridge 2 to 1. Under a set of dc voltages of $V_{D1} = 320$ V and $V_{D2} = 180$ V, the power transfer P_D was limited below 5 kW as shown in Fig. 10. The peak current $I_{1\text{peak}}$ was 60 A in Fig. 12, as calculated in this section.

VII. Application to an Energy Storage System with Galvanic Isolation

A. A 200-V, 10-kW, 2.6-kJ Laboratory Model

Fig. 13 depicts the experimental energy storage system rated at 200 V, 10 kW, and 2.6 kJ. Circuit parameters in the dc/dc converter were the same as those in Table I. An electrolytic capacitor bank C_{ES} of 60,000 μF was used in the experiment to simulate an EDLC bank. The voltage across the capacitor bank is charged up to 350 V and discharged down to 190 V. Thus, an energy of 2.6 kJ is stored into, and released out of, the capacitor bank. It corresponds to 70% of the energy stored in C_{ES} at 350 V. The three-phase PWM converter regulates v_{D1} at 320 V. Its PWM carrier frequency was 10 kHz.

B. Charging and Discharging of the Capacitor Bank

Fig. 14 shows the experimental waveforms when the energy storage capacitor bank C_{ES} was repetitively charged up to 350 V, and then discharged down to 190 V. The waveform of i_{D2} was observed via a low-pass filter with a cut-off frequency of 800 Hz. The maximal power transfer was 9.3 kW. In this experiment, the phase shift δ had a square waveform with an amplitude of 30° to make the controller in the experimental system simple. In actual energy storage systems, however, the power transfer P_D should be determined by power demand, or a higher-level controller regulating the voltage on the utility grid.

VIII. Starting Procedure

At the starting of the system, if bridge 1 produced a square voltage of v_1 at $v_{D1} = 320$ V and $v_{D2} = 0$ V, an inrush current would flow into the auxiliary inductors L_a and the transformer. The inrush current would result in magnetic saturation in the cores of L_a, leading to an even larger inrush current. Hence, a special operation mode called "precharging operation" is presented and described to charge the capacitor bank from zero to the rated voltage of 320 V, preventing such an inrush current from flowing. The precharging operation allows the energy storage system to require no external starting-up or precharging circuit.

Fig. 15 shows the starting-up and precharging transient waveforms of the dc/dc converter when the capacitor bank began being charged from zero to 320 V. In this experiment, v_{D1} had been already charged up to 320 V before the dc/dc converter started the precharging operation. Bridge 1 produced a voltage v_1 with a duty ratio of $d = 20\%$ rather than 100% while bridge 2 was operated as a diode rectifier with all the IGBTs kept off. The first pulse of v_1 had a half duty ratio of $d/2 = 10\%$ to suppress dc magnetization of the transformer. The peak current at the first pulse of v_1, I_{1pp} is expressed as

$$I_{1pp} = \frac{\pi V_{D1}}{\omega L}\frac{d}{2}. \tag{18}$$

In Fig. 15, the negative peak current reached 30 A, while its theoretical value was 19.2 A.

Fig. 16 shows the experimental waveforms of the dc voltage, current, and power. The starting procedure took approximately eight seconds to charge the capacitor bank from zero to 320 V. No excessive inrush current flowed into the capacitor bank. When v_{D2} reached 275 V, the dc/dc converter changed its operation mode from the precharging operation to the normal operation with the square voltages of v_1 and v_2 having no phase shift ($d = 100\%$ and $\delta = 0°$). The power transfer P_D in the normal operation at $\delta = 0°$ has a negative-feedback effect to balance the two dc voltages v_{D1} and v_{D2} due to the existence of the dead time T_d. Therefore, after v_{D2} reached 275 V, it was naturally charged up to the same voltage as v_{D1}.

IX. Conclusions

This paper has addressed an bi-directional isolated dc/dc converter suitable for an energy storage system. Theoretical calculations of power losses and peak current have clarified the dc-voltage limitations in the energy storage system. Experimental results have revealed that the dc/dc converter can charge and discharge the capacitor bank properly. Moreover, the dc/dc converter can charge the capacitor bank from zero to the rated voltage without any external precharging circuit.

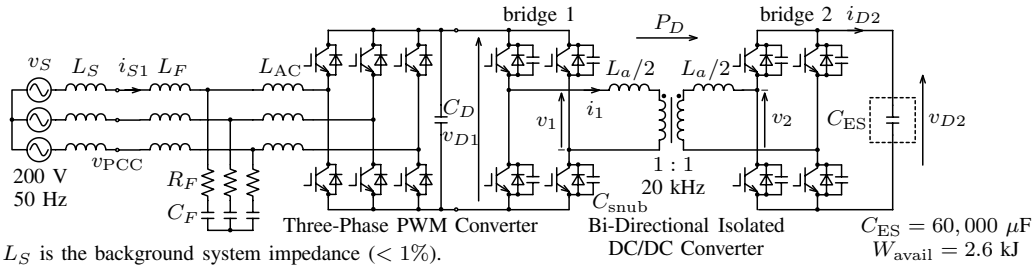

L_S is the background system impedance ($< 1\%$).
$L_{\rm AC} = 280\ \mu$H (2.2%), $L_F = 44\ \mu$H (0.34%),
$R_F = 0.2\ \Omega$ (5%), $C_F = 150\ \mu$F (20%), based on 200 V, 10 kW, and 50 Hz.

Fig. 13. A 200-V, 10-kW experimental circuit with energy-storage electrolytic capacitors of 60,000-μF to simulate an EDLC bank.

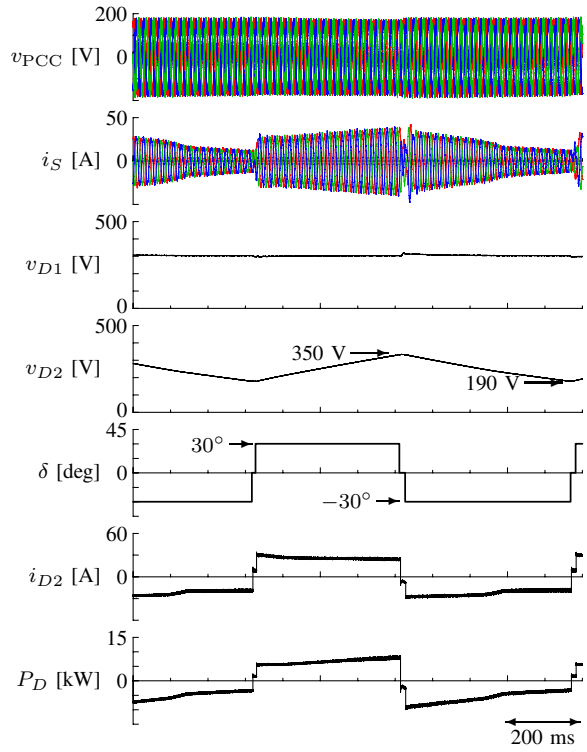

Fig. 14. Experimental waveforms of charging and discharging of the capacitor bank ($W_{\rm avail} = 2.6$ kJ)

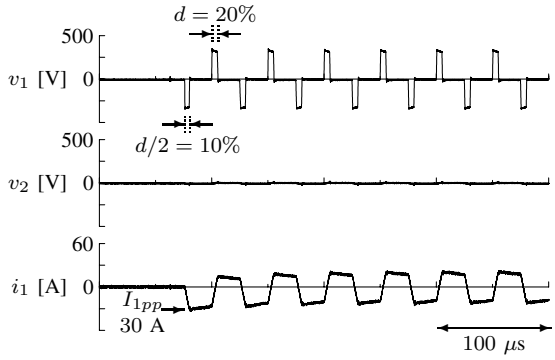

Fig. 15. Transient waveforms when the dc/dc converter starts precharging the capacitor bank.

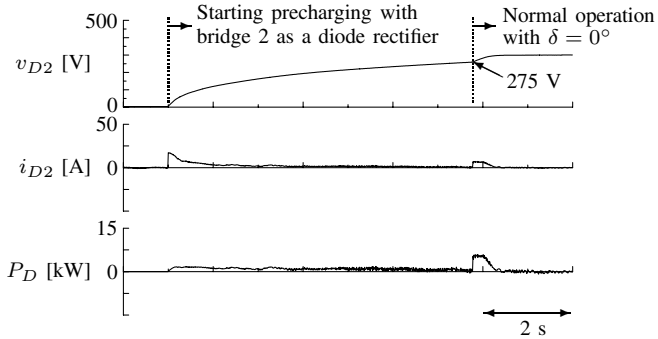

Fig. 16. Experimental waveforms of the dc voltage, current, and power in the precharging period.

REFERENCES

[1] P. F. Ribeiro, B. K. Johnson, M. L. Crow, and A. Arsoy, and Y. Liu, "Energy storage systems for advanced power applications," *Proceedings of the IEEE*, vol. 89, issue 12, pp. 1744-1756, 2001

[2] T. Kinjo, T. Senjyu, N. Urasaki, and H. Fujita, "Output levelling of renewable energy by electric double layer capacitor applied for energy storage system," *IEEE Trans. Energy Convers.*, vol. 21, no. 1, pp. 221-227, 2006

[3] M. Jain, M. Daniele, P. K. Jain, "A bidirectional dc-dc converter topology for low power application," *IEEE Trans. Power Electron.*, vol. 15, no. 4, pp. 595-606, 2000

[4] T. Kohama, M. Yamashima, and T. Nishimiya, "Operation-mode control of active-clamped bi-directional flyback converter as EDLC charger and discharger," *PCC-Osaka 2002*, vol. 3, pp. 1155-1159, 2002

[5] A. D. Swingler and W. G. Dunford, "Development of a bi-directional dc/dc converter for inverter/charger applications with consideration paid to large signal operation and quasi-linear digital control," *PESC 2002*, vol. 2, pp. 961-966, 2002

[6] F. Z. Peng, H. Li, G.-J. Su, and J. S. Lawler, "A new ZVS bi-directional dc-dc converter for fuel cell and battery application," *IEEE Trans. Power Electron.*, vol. 19, no. 1, pp. 54-65, 2004

[7] L. Zhu, "A novel soft-commutating isolated boost full-bridge ZVS-PWM dc-dc converter for bi-directional high power applications," *IEEE Trans. Power Electron.*, vol. 21, no. 2, pp. 422-429, 2006

[8] L. Shi, L. Sun, D. Xu, and M. Chen, "Optimal design and control of 5 kW PWM plus phase-shift (PPS) control bidirectional dc-dc converter," *APEC 2006*, CD-ROM, 2006

[9] Y. Hu, J. Tatler, and Z. Chen, "A bi-directional dc/dc power electronic converter for an energy storage device in an autonomous power system," *IPEMC 2004*, vol. 1, pp. 171-176, 2004

[10] R. W. De Doncker, D. M. Divan, and M. H. Kheraluwala, "A three-phase soft-switched high-power density dc/dc converter for high-power applications," *IEEE Trans. Ind. Applicat.*, vol. 27, no. 1, pp. 63-73, 1991

[11] M. H. Kheraluwala, R. W. Gascoigne, and D. M. Divan, "Performance characterization of a high-power dual active bridge dc-to-dc converter," *IEEE Trans. Ind. Applicat.*, vol. 28, no. 6, pp. 1294-1301, 1992

[12] S. Inoue and H. Akagi, "A bi-directional isolated dc/dc converter as a core circuit of the next-generation medium-voltage power conversion system," *PESC 2006*, CD-ROM, 2006, (to be published in the *IEEE Trans. Power Electron.*)

[13] M. Pavlovsky, S. W. H. de Haan, and J. A. Ferreira, "Concept of 50 kW DC/DC converter based on ZVS, quasi-ZCS topology and integrated thermal and electromagnetic design," *EPE 2005*, CD-ROM, 2005